crystals

MDPI

Article

Domain Patterning in Ion-Sliced $LiNbO_3$ Films by Atomic Force Microscopy

Tatyana Volk [1,*], Radmir Gainutdinov [1] and Haihua Zhang [2]

[1] Shubnikov Institute of Crystallography of FSRC "Crystallography and Photonics" RAS, Moscow 119333, Russia; rgaynutdinov@gmail.com
[2] Jinan Jingzheng Electronics Co. Ltd., Jinan 250101, China; cathy@nanoln.com
* Correspondence: volk@crys.ras.ru; Tel.: +7-499-135-6100

Academic Editor: Maria-Pilar Bernal
Received: 7 April 2017; Accepted: 11 May 2017; Published: 14 May 2017

Abstract: Photonic structures denoted as LNOI ($LiNbO_3$-on-insulator) are of considerable interest for integrated optics due to a high refractive-index contrast provided by the interface $LiNbO_3$/insulator. A topical problem for LNOI-based optical waveguides is optical-frequency conversion, in particular realized on ferroelectric domains on the basis of quasi phase-matching principle. This paper presents extended studies on the fabrication of domain patterns by atomic force microscopy (AFM) methods (raster lithography, piezo-force microscopy, conductive AFM) in single-crystal ion-sliced $LiNbO_3$ films forming LNOI sandwiches. A body of data obtained on writing characteristics of domains and specified 1D and 2D domain patterns permitted us to manipulate the domain sizes and shapes. Of special importance is the stability of created patterns, which persist with no degradation during observation times of months. The domain coalescence leading to the transformation of a discrete domain pattern to a continuous one was investigated. This specific effect—found in thin $LiNbO_3$ layers for the first time—was attributed to the grounding of space-charges accumulated on domain walls. Observations of an enhanced static conduction at domain walls exceeding that in surrounding areas by not less than by five orders of magnitude supports this assumption. AFM domain writing in ion-sliced films serves as a basis for studies in nonlinear photonic crystals in integrated optical schemes.

Keywords: Lithium niobate; LNOI; ferroelectric domains; domain-wall conduction; AFM

1. Introduction

Lithium niobate is the key material for integrated photonics/optics due to a unique combination of excellent optical, acousto-, and nonlinear-optical properties demanded by integrated devices. Over the past decade, the manufacture of thin (hundreds of nanometers thick) single-crystal LiNbO3 films was elaborated with the use of ion-slicing technology [1]. Sandwich structures fabricated by bonding ion-sliced single-crystal $LiNbO_3$ films to insulator substrates—denoted as LNOI ("lithium niobate-on-insulator")—have attracted considerable interest. Physical phenomena and fundamental technologies underlying the fabrication of ion-sliced $LiNbO_3$ films, methods of bonding them to various insulating substrates, and relevant bibliography can be found, for example, in reviews [2,3]. An interest in LNOI structures is primarily because embedding a $LiNbO_3$ film in a low refractive-index insulator substrate provides a high-index-contrast optical waveguide.

Some encouraging results were obtained in studies of LNOI-based optical elements, such as photonic crystals [4,5], high-Q microresonators [6–8], ridge-waveguides [9,10], proton-exchanged waveguides [11–13] and modulators [14], hybrid lightwave circuits LNOI-SOI [15], etc. These results indicate that LNOI is an appropriate platform for integrated optics.

A typical problem for LNOI-based waveguides is the nonlinear-optical frequency conversion, which can be realized on the basis of either phase-matching (PM) or quasi-phase-matching (QPM) principles. In the latter case, an artificially created ferroelectric domain pattern serves as a frequency convertor. Traditionally, periodically-poled $LiNbO_3$ (PPLN) elements are produced by the application of external fields to an electrode pattern deposited onto the crystal surfaces. Alternative methods such as domain writing by atomic force microscope (AFM)-tip voltages or electron-beam of SEM permit the creation of domain patterns up to the nanoscale (e.g., [16]). To fabricate ion-sliced PPLN films, the authors of [17,18] applied the technique of ion-slicing to a bulk PPLN plate. At the same time, the abovementioned non-contact microscopic methods of domain fabrication are especially appropriate for use in thin layers, since in this case an undesirable decrease of the field across the layer thickness and resulting domain-wall inclination observed in crystal plates (e.g., [16]) are negligible.

In [19] we reported on domain writing by dc AFM-tip voltages in ion-sliced $LiNbO_3$ films forming LNOI. 2D domain patterns were written—both discrete (consisting of isolated domains up to the nanoscale) and arbitrary-shaped continuous ones. All patterns were completely stable and revealed no degradation in real-time. These results promise LNOI structures to be a platform for studies in nonlinear photonic crystals [20]. The authors of [21] reported the fabrication of stable domain patterns in LNOI sandwiches by applying external fields. A specific feature of the domain evolution found by us [19] was the coalescence of adjacent domains as the distance between them was decreased (this coalescence occurring in an array of isolated domains has no relation to the domain coalescence terminating the polarization reversal under uniform external fields).

In this connection, the writing of nanodomain arrays in ion-sliced $LiNbO_3$ films is of interest in the context of high-density data storage in ferroelectrics [22,23]. The authors of [24,25] reported on the writing of nanodomain patterns in ultrathin single-crystal $LiTaO_3$ plates. The minimum domain-dot diameter of 6 nm together with the inter-domain distance of about tens of nm provided a memory density as high as 1–10 Tbits in^2. In these works, contrary to our results [19], no domain coalescence was mentioned. So, the question arises as to which factors promote or suppress domain coalescence and how it can influence the tolerable interdomain spacing (i.e., the storage density).

The ion-sliced films under study seem to be an appropriate medium for investigations of ferroelectric phenomena—specifically of domain formation—in $LiNbO_3$ films and thin layers as a whole. This paper presents extended studies of these subjects started in [19].

Our experiments were performed in LNOI samples provided by Nanoln Electronics (Jinan, China).

2. Results and Discussion

The schematic diagram of our experiments is shown in Figure 1. Figure 1a,b display two types of samples (S1 and S2) under study and the scheme of AFM domain writing. Methods of domain fabrication and investigation with the use of scanning probe microscopy are described, for example, in [26]. Figure 1c illustrates the domain state of samples after applying AFM dc-voltages; the spontaneous polarization directions P_{up} and P_{down} correspond to the initial and reversed states, respectively; the reversal from P_{up} to P_{down} occurs under positive $+U_{tip}$.

Samples of S1 type are composed of a +Z-cut ion-sliced single-domain $LiNbO_3$ film bonded to a SiO_2-coated $LiNbO_3$ wafer. An Au/Cr layer is incorporated between the bottom film surface and SiO_2 layer. Sample 2 is composed of a +Z cut ion-sliced single-domain $LiNbO_3$ film bonded directly to a SiO_2-coated $LiNbO_3$ wafer without a metal interlayer.

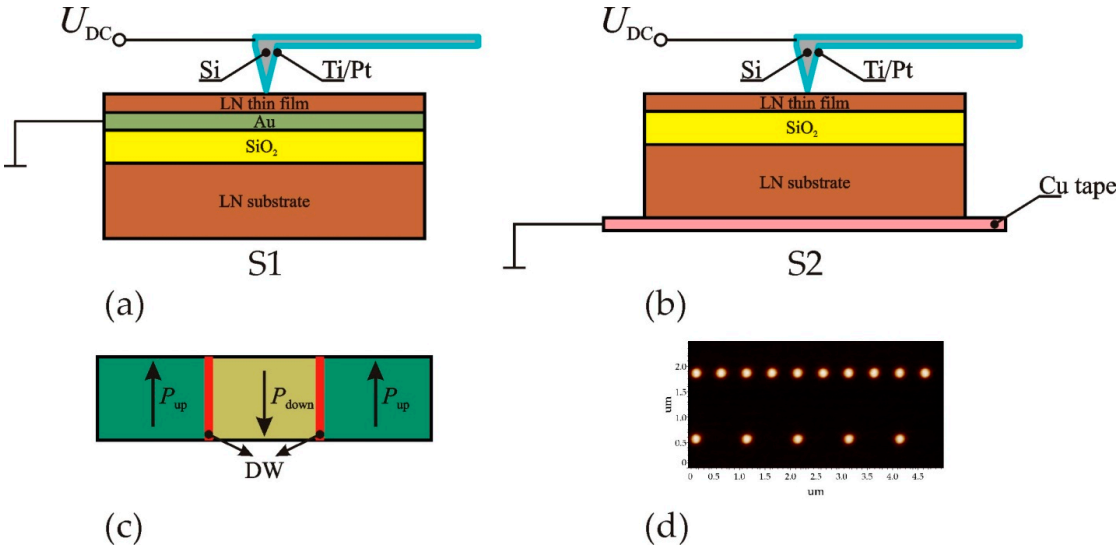

Figure 1. Schematic presentation of an atomic force microscope (AFM)-tip domain writing in samples (**a**) S1 and (**b**) S2 and (**c**) the written domains (P_{up} and P_{down} show the initial and reversed polarization, respectively, DW denotes domain walls); (**d**) exemplifies isolated domains written by Utip = 50 V, tp = 0.1 ms.

2.1. Writing of Isolated Domains

In this section, we briefly characterize the dependences of domain formation on the exposure conditions. Figure 1d exemplifies piezoelectric force microscopy (PFM) images of written isolated domains. The minimum achieved domain diameter D, determined by the tip radius R, is 50 nm. D linearly grows with U_{tip} at a given t_p (Figure 2a). Domains appear after the application of certain threshold tip-voltage U_{thr}, which decreases with growing pulse duration (Figure 2b). So, for a given U_{tip}, a certain pulse duration is required to retain formed domains, whereas they decay at shorter t_p. This is a manifestation of a backswitching effect which is characteristic of $LiNbO_3$ [16].

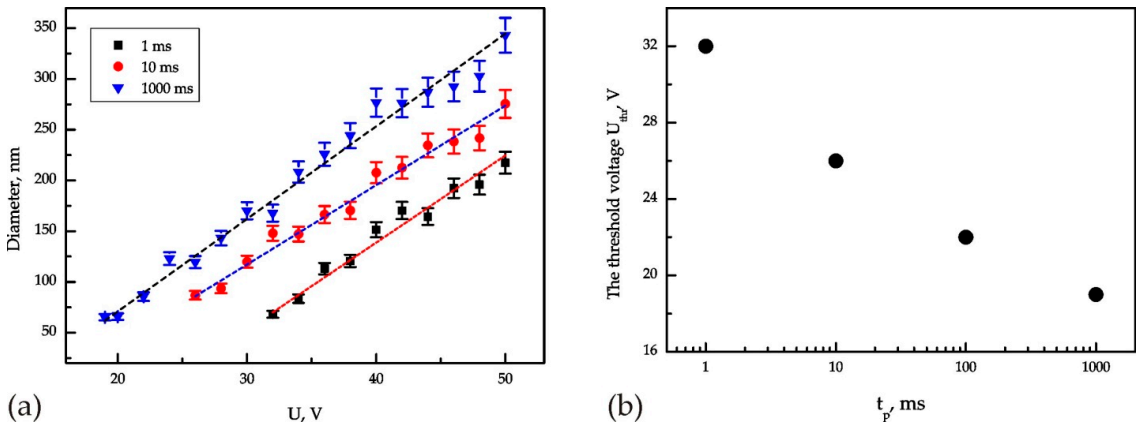

Figure 2. (**a**) Domain diameter vs. voltage for t_p = 1, 10 and 1000 ms (squares, circles, and triangles, respectively); (**b**) the threshold voltages of domain appearance at different exposure times.

The linear dependences $D(U_{tip})$ qualitatively resemble those reported, for example, for AFM-domain writing in thin stoichiometric $LiNbO_3$ crystals [27–29]. On the contrary, the exposure dependences of the domain diameter at U_{tip} = const differ markedly from $D(t_p)$ reported earlier [27–29], and are worthy of a more detailed discussion.

Figure 3a shows D(t_p) in the logarithmic scale for different tip voltages. The domain diameter grows up to a salient point, whereupon it comes to a plateau. These curves are fundamentally different from linear D(t_p) in ultrathin $LiNbO_3$ crystals [28]. Following the method proposed in [30], we calculated the average velocity of the domain widening (i.e., the sideways domain-wall (DW) velocity V_{DW}) against the domain diameter D. The velocity was taken from D(tp) as $V_{DW} = \Delta D_i/\Delta t_i$, where ΔD_i is the increment of D in a time Δt. The obtained nonmonotonic curves V_{DW}(D) are displayed in Figure 3b. Comparison of Figure 3a,b shows that a "saddle" in curves D(t_p) corresponds to a sharp slowing-down (practically, to stopping) of DW motion. Based on the approach of [30], which models the AFM tip as a sphere, we evaluated the axial fields E at the domain boundaries. For salient points in Figure 3a these estimates give E of 0.26 10^8 V/m and 0.29 10^8 V/m, respectively, for U_{tip} = 35 V and 50 V. These values are rather close to the coercive field Ec = 0.22 10^8 V/m in $LiNbO_3$ bulk crystals. Despite the approximate nature of these estimates, this result seems to be not occasional and permits us to interpret the saddles in D(t_p) curves (Figure 3a) as a threshold-like slowing down of the sideways DW motion just at that distance D from the tip contact-point, at which the field drops below E_c.

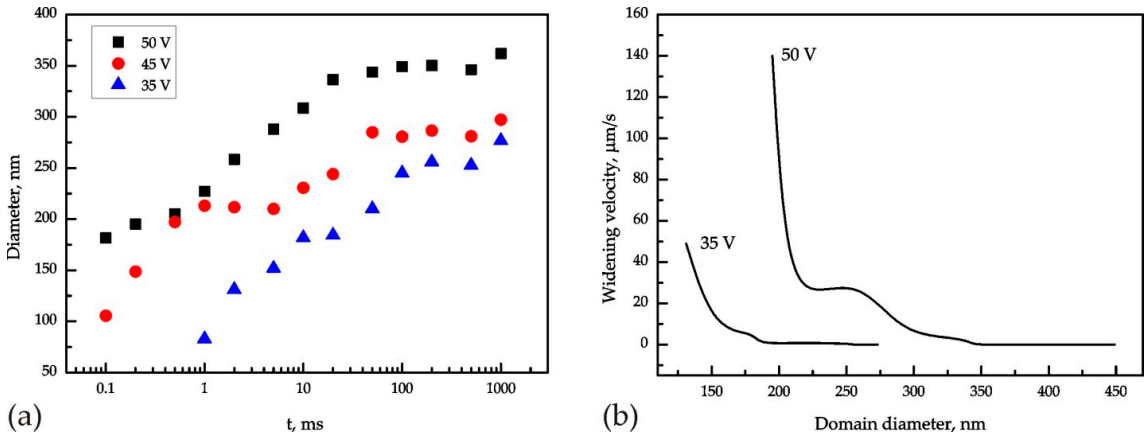

Figure 3. (**a**) Domain diameter versus exposure time for U_{tip} = 35, 45, and 50 V (denoted by triangles, circles, and squares, respectively); (**b**) Velocity of domain widening against the domain diameter for 35 and 50 V (the left and right curves, respectively).

2.2. Specific Formation of Domain Patterns in Ion-Sliced $LiNbO_3$ Films

2.2.1. Coalescence of Domains

As mentioned above, the closely spaced domains tend to coalesce [19]. Here we present the extended investigations of this effect (Figure 4). In samples S1 (Figure 1a), domain chains (Figure 4a,b) and domain squares (Figure 4c–f) were written by means of step-by-step in-plane displacements of the tip by a specified distance Λ. For a given pattern, Λ is constant; in the written squares, Λ along the both sides are equal.

Figure 4a,d demonstrate the evolution (bottom-up) of a domain chain as Λ decreases from 1000 to 100 nm (for all chains U_{tip} = 50 V, t_p = 1 ms). Figure 4b,e and Figure 4c,f display images of the discrete and continuous domain squares written with Λ = 500 and 200 nm, respectively (U_{tip} = 50 V, t_p = 10 ms). Both the discrete domain chain and square transform to unbroken ones. PFM amplitude images of terminating continuous patterns (the upper rows of Figure 4d and the square in Figure 4f) reveal inboard no traces of domain boundaries, appearing as dark contours. In other words, the domain coalescence leads to the formation of a large completely uniform 2D domain. All written patterns—both discrete and continuous—are completely stable for up to several months.

The coalescence is determined by only the distance between DWs, and does not depend on the domain sizes. Rough estimates based on the examination of chains with varied domain diameter permit us to conclude that the coalescence occurs if the inter-domain distance becomes lesser than

20–30 nm. Interestingly, this "critical" value is on the same order of magnitude as the inter-domain distances in nanodomain patterns, providing an ultrahigh storage density in $LiTaO_3$ films [24,25].

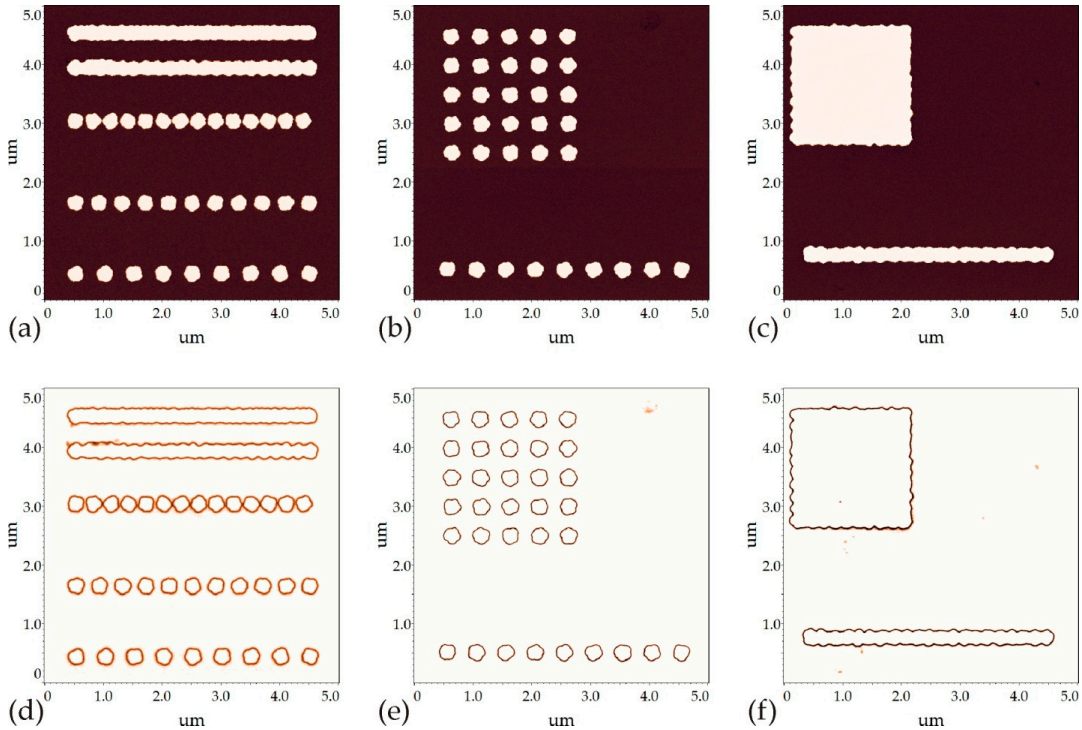

Figure 4. Transformation of discrete domain patterns to continuous ones; the upper and lower rows present, respectively, phase and amplitude piezoelectric force microscopy (PFM) images of written patterns. (**a**,**d**)—domain chains written with decreasing distance Λ between writing points: Λ = 500, 400, 300, 200, and 100 nm (bottom-up); (**b**,**e**) and (**c**,**f**)—domain squares written with Λ = 500 and 200 nm, respectively.

The domain sizes are unaffected by the inter-domain spacing; e.g., in the discrete domain chains displayed in three lower rows of Figure 4a,b, the domain diameters are the same to within 1%, as is the width of the continuous domain line (the upper rows in Figure 4a,b).

Figure 5a,b present PFM images of domain gratings written in a sample S1 by raster lithography. The grating periods are Λ = 300 and 2000 nm, the grating sizes are of 4 × 4 μm^2 and 20 × 20 μm^2, the total times of writing of the smaller and larger patterns were 30 and 300 s, respectively. The patterns are rather regular with the off-duty ratios of 0.5 and 0.6, respectively. Figure 5c shows a PFM image of an arbitrary-shaped domain pattern written in S1; the reversed domain areas are dark. A compliance of samples S1 to shaping of domain patterns of any specified design seems to be akin to the effect of domain coalescence described above.

The coalescence of closely-spaced domains in sample S1 has not been reported before and disagrees with the data reported on AFM domain writing in $LiNbO_3$. In thin $LiNbO_3$ crystals [31], a domain instability was observed as the inter-domain spacing was decreased. In thin He-implanted $LiNbO_3$ layers, a reduction of the inter-domain spacing was accompanied by a decrease of the domain diameter [32]. These effects were interpreted as a consequence of the inter-domain electrostatic repulsion. While writing domain chains in thin $LiNbO_3$ crystals [33], no domain coalescence was observed. By contrast, chaotic discrete patterns appeared as the chain links were reduced.

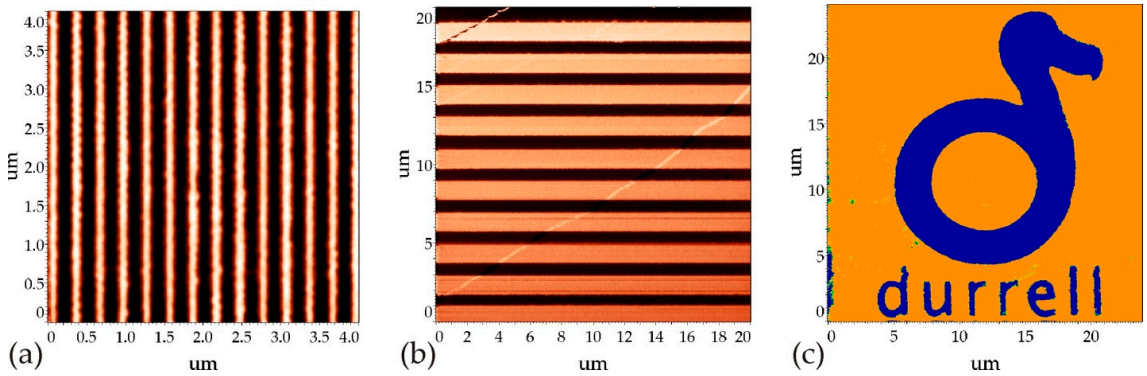

Figure 5. (**a**–**c**): phase PFM images of domain gratings and of an arbitrary-shaped pattern written in samples S1 by raster lithography. Periods of the left and right gratings are Λ = 300 and 2000 nm, respectively, the bright contrast corresponds to the switched stripes. In (**c**) the dark contrast corresponds to the switched areas.

2.2.2. Relation of Domain Coalescence to the Domain-Wall Conduction

The domain coalescence evidences the freedom from electrostatic repulsion between the adjacent domains. According to the approach developed recently [34–37], DWs represent the areas of an enhanced conduction owing particularly to a charge accumulation/depletion, which is caused by a variety of reasons. Intuitively, we related the domain coalescence to effects of an enhanced conduction at DWs. To support this assumption, research into the conduction at DWs was performed.

Domain-wall conduction (DWC) in $LiNbO_3$ was recently investigated in (15–500)-μm-thick plates [38–40]. The first studies of DWC in thin LiNbO3 films were performed recently by us [41]. The conduction was measured in domain gratings with the period Λ= 3.6 μm. For clarity, the results of these measurements discussed in detail in [41] are shown schematically in Figure 6.

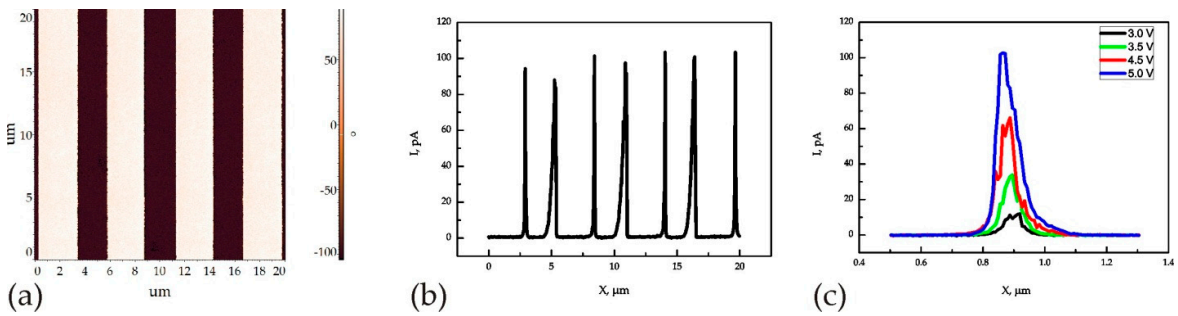

Figure 6. Schematic presentation of the domain-wall conduction in a written domain grating. (**a**) PFM phase image of a domain grating with Λ = 3.6 μm; (**b**) a line profile of conductive atomic force microscopy (C-AFM) map exemplifies current anomalies observed at DWs; the current peaks I_{max} under Utip ≤ 5 V are in the range of 20–100 pA, whereas away from DWs I_{max} < 0.03 pA (the sensitivity of our equipment); (**c**) I_{max} in a fixed DW point vs. U_{tip}.

Figure 6a,b display, respectively, a PFM phase image of a written grating and a line profile of currents measured by conductive atomic force microscopy (C-AFM) method; current peaks I_{max} are observed at DWs. Figure 6c illustrates an increase of I_{max} with increasing measuring voltage U_{tip} (the measuring voltage is positive, thus directed along P_{up}). The current peaks at DWs persist during observation times of up to several months; i.e., their steadiness is determined by the stability of the written patterns. Studies in piezoelectric hysteresis loops presented in [41] permitted us to unambiguously relate these currents to a static DWC. Preliminary estimates have shown [41] that the conduction at DWs is at least five orders of magnitude higher than in surrounding areas.

The existence of an enhanced static conduction at DWs permits one to regard them as stable conducting wires embedded into an insulating matrix. As mentioned above, there is evidence of an electrostatic repulsion between closely-spaced domains in $LiNbO_3$ [31,32], which is evidently related to charge accumulation at DWs. We assume that domain coalescence in sample S1 is due to the grounding of space charges accumulated at DWs through the bottom metal interlayer.

To support this assumption, we performed writing of domain chains in sample S2. The fundamental distinction of sample S2 (Figure 1b) from sample S1 (Figure 1a) is the absence of a metal interlayer between $LiNbO_3$ film and the insulating SiO_2 substrate.

Figure 7 presents the formation of domain chains written in sample S2 by the same procedure as in S1. The observed domain evolution is dramatically different from that in S1 (Figure 4). In Figure 7a–c, PFM phase images present the chains written with decreasing distances Λ between the writing points (bottom-up); Λ was reduced from 1000 to 100 nm. The images shown in Figure 7a–c were obtained at 6, 12, and 24 min subsequent to writing.

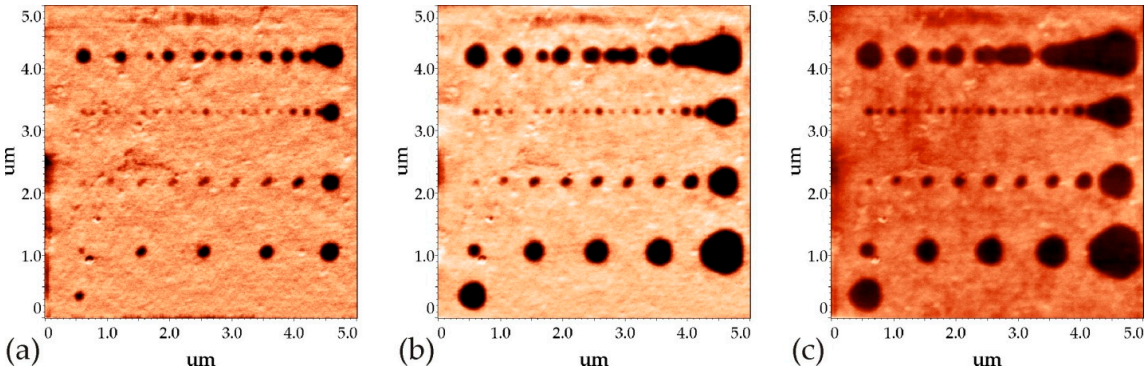

Figure 7. Evolution of domain chains written in sample S2, subsequent to writing. PFM phase images (**a**–**c**) were obtained in 6, 12, and 24 min, respectively, subsequent to writing. The chains were written with the distances between writing points Λ = 1000, 500, 200, 100 nm (bottom-up).

As can be seen, the fundamental distinctions of the domain formation in S2 from that in S1 are first an irregularity and discreteness of all written patterns, and second, their instability. The domain diameter decreases from the chain "heads" (the starting writing points) to "tails" (from right to left in Figure 7a,b). At minimum specified distances between the writing points, a chain remains discrete. On turning-off U_{tip}, the chains rearrange over the course of tens of minutes, coming to a stable shape which then persists in real-time. The observed irregular patterns qualitatively resemble chaotic patterns appearing at short inter-domain distances when writing domain chains in thin $LiNbO_3$ crystals [33]. These effects were interpreted as a manifestation of screening with emphasis on the humidity influence [33]. A fundamental difference in domain formation in samples S1 and S2 cannot be interpreted in this framework, since all results described above were obtained at an identical humidity of 40%.

The attempts made to write domain gratings by raster lithography in sample S2 failed, since the arising patterns were irregular and quite unstable. This ruled out the possibility of measurements of DWC in S2.

The difference in domain formation in samples S1 and S2 supports our assumption that in S1 the charges accumulated at DWs are grounded through the metal inter-layer. This grounding eliminates the inter-domain electrostatic repulsion, which impedes the domain coalescence. Additionally, it assists in the establishment of charge equilibrium. Stable domain patterns in sample S1 are observed immediately on writing (i.e., the charge equilibrium is achieved instantaneously). In S2, a slow rearrangement of written patterns to stable shapes occurs over the course of tens of minutes (Figure 7), which evidently means a slow approach to equilibrium.

Our conclusion concerning the grounding through DWs is still qualitative and requires deeper investigations. At the same time, it is consistent with the observations mentioned in [38,39], according to which DWs serve as *"nanoscale vias"* assisting in controlled domain fabrication.

We comment qualitatively on the observed static DWC. Until recently, it was attributed to the accumulation of a screening charge on inclined domain walls (e.g., [42]). In particular, a static conductivity observed in domain patterns of various orientation fabricated in (15–500)-μm-thick $LiNbO_3$ plates [38,39] was unambiguously accounted for by this model. However, the results presented in [41] and cited here differ fundamentally from [38,39] because the currents observed in [38,39] only appeared under a photoactive illumination. This means that an ultra-low dark conductivity of $LiNbO_3$ could not provide a sufficient charge density at DWs in darkness. A drastic jump of the conduction at DWs observed in our case is obviously related to reasons other than the screening of macroscopically inclined domain walls. The number of approaches to the DWC grows permanently, but no general model has been proposed so far. For example, recent experiments in periodically-poled $LiNbO_3$ [43] have shown that 180° DWs in these artificially created domain patterns are essentially meandered, and contain local inclinations and even head-to-head or tail-to-tail local configurations. A local charging of DWs occurring at these nonunformities might be responsible for DWC.

Interestingly, the charge accumulation/depletion at DWs in oxide ferroelectrics are usually discussed in the framework of the dominant role of oxygen vacancies (e.g., [34,37]). According to the current concept of the $LiNbO_3$ intrinsic defect structure [16], congruently melting $LiNbO_3$ (CLN) crystals are free of O-vacancies, so the microscopic mechanism of DWC in this material can be related to quite different charge-transport schemes.

3. Materials and Methods

The samples under study were produced of congruently melting $LiNbO_3$ (CLN). Ion-sliced z-cut CLN films forming S1 and S2 samples were either 0.5 or 0.3 μm thick. In sample S1 (Figure 1a), the Au/Cr layer incorporated between the bottom film surfaces and the SiO_2 layer was 100 nm thick. In all samples, the SiO_2 layer was 1.4 μm thick. All samples were of the total size X × Y × Z = 11 × 9 × 0.5 mm^3.

The local polarization reversal was induced by applying dc-voltages to a conductive AFM tip contacting the sample surface. To create isolated domains, dc-voltage with a given magnitude U_{tip} and rising pulse duration t_p (or, vice versa, with a fixed t_p and rising U_{tip}) was applied step-by-step to the tip, U_{tip} and t_p ranging from 0 to 50 V and from 0.1 to 1000 ms, respectively. At each step, this surface region was scanned by piezoelectric force microscopy (PFM). Based on these data, the dependences $D(U_{tip})$ for t_p = const and $D(t_p)$ for U_{tip} = const were constructed. 2D domain patterns were written by raster lithography method with graphic templates, whereupon they were examined by PFM scanning. PFM amplitude and phase images of written patterns were obtained by measuring the electromechanical response signal H_f.

$$H_f = \left[\frac{1}{k}\frac{dC}{dz}\left(\frac{V^{\uparrow} + V^{\downarrow}}{2}\right) \mp d_{33}\right] U_{ac}$$

where d_{33} is the piezoelectric coefficient; k is the force constant of the tip, C is the tip–sample capacity, $\left(\frac{V^{\uparrow}+V^{\downarrow}}{2}\right)$ is the average contact potential difference between the tip and the crystal surface, and U_{ac} is the ac voltage between the tip and the electroded counter surface. PFM images consist of x-y maps of the amplitude and phase PFM signal. The conduction in the domain gratings written by raster lithography method was measured by the conductive atomic force microscopy (C-AFM). C-AFM maps were obtained by applying positive bias voltages U_{tip} in the range from 2 to 5 V between the grounded conductive tip and the Cr/Au interlayer.

All AFM experiments were carried out with an NTEGRA PRIMA AFM (NT–MDT, Moscow, Russia). Si probes with Pt conducting coating (SPM-PIT, Bruker, Billerica, USA) were utilized; the tip radius R = 20 nm and 50 nm, the cantilever stiffness k ~2.8 N/m, and resonance frequency f ~75 kHz.

4. Conclusions

In summary, we have shown that domain writing by AFM-tip voltages in ion-sliced LiNbO3 films permits the manipulation of the sizes and shapes of written stable patterns in wide limits from nanosized domain dots to large (of tens of microns) arbitrarily-shaped patterns by means of varying the exposure conditions and interdomain spacing. The compliance of these films to domain patterning make them an appropriate laboratory medium for studies on the fabrication of nonlinear photonic crystals [20] and optical-frequency conversion on them. Additionally, studies in AFM-domain writing in these films can be helpful for analyzing the factors determining storage density in memory systems based on domain writing in thin layers.

Acknowledgments: This work was supported by the Russian Foundation for Basic Researches, Projects Nos. 16-29-11777_ofi_m and 16- 02-00439a. The equipment of the Shared Research Center supported by the Ministry of Education and Science (Project No. RFMEFI62114X0005) was used in experiments.

Author Contributions: Tatyana Volk analyzed the data and wrote the paper, Radmir Gainutdinov performed the experiments and analyzed the data, Haihua Zhang provided with the samples.

Conflicts of Interest: The authors declare no conflict of interest.

References

1. Levy, M.; Osgood, R.M.; Liu, R.; Cross, L.E.; Cargill, G.S., III; Kumar, A.; Bakhru, H. Fabrication of single-crystal lithium niobate films by crystal ion slicing. *Appl. Phys. Lett.* **1998**, *73*, 2293–2295. [CrossRef]
2. Hu, H.; Yang, J.; Gui, L.; Sohler, W. Lithium Niobate-on-insulator (LNOI): Status and perspectives. *Proc. SPIE* **2012**, *8431*, 84311D. [CrossRef]
3. Poberaj, G.; Hu, H.; Sohler, W.; Guenter, P. Lithium niobate on insulator (LNOI) for micro-photonic devices. *Laser Photonics Rev.* **2012**, *6*, 488–503. [CrossRef]
4. Lu, H.; Sadani, B.; Courjal, N.; Ulliac, G.; Smith, N.; Stenger, V.; Collet, M.; Baida, F.I.; Bernal, M.P. Enhanced electro-optical lithium niobate photonic crystal wire waveguide on a smart-cut thin film. *Opt. Exp.* **2012**, *20*, 2974–2981. [CrossRef] [PubMed]
5. Li, Y.; Wang, C.; Loncar, M. Design of nano-groove photonic crystal cavities in lithium niobate. *Opt. Lett.* **2015**, *40*, 2902–2905. [CrossRef] [PubMed]
6. Wang, R.; Bhave, S.A. Free-standing high quality factor thin-film lithium niobate micro-photonic disk resonators. *arXiv Prepr.* 2014; arXiv:1409.6351.
7. Wang, J.; Bo, F.; Wan, S.; Li, W.; Gao, F.; Li, J.; Zhang, G.; Xu, J.J. High-Q lithium niobate microdisk resonators on a chip for efficient electro-optic modulation. *Opt. Exp.* **2015**, *23*, 23072–23078. [CrossRef] [PubMed]
8. Lin, J.; Xu, Y.; Fang, Z.; Wang, M.; Song, J.; Wang, N.; Qiao, L.; Fang, W.; Cheng, Y. Fabrication of high-Q lithium niobate microresonators using femtosecond laser micromachining. *Sci. Rep.* **2015**, *5*, 8072. [CrossRef] [PubMed]
9. Rabiei, P.; Steier, W.H. Lithium niobate ridge waveguides and modulators fabricated using smart guide. *Appl. Phys. Lett.* **2005**, *86*, 161115. [CrossRef]
10. Volk, M.F.; Suntsov, S.; Rüter, C.E.; Kip, D. Low loss ridge waveguides in lithium niobate thin films by optical grade diamond blade dicing. *Opt. Exp.* **2016**, *24*, 1386–1391. [CrossRef] [PubMed]
11. Cai, L.; Li, S.; Han, H.; Hu, H. Waveguides in single-crystal lithium niobate thin film by proton exchange. *Opt. Exp.* **2015**, *23*, 1240–1248. [CrossRef] [PubMed]
12. Cai, L.; Wang, Y.; Hu, H. Low-loss waveguides in a single-crystal lithium niobate thin film. *Opt. Lett.* **2015**, *40*, 3013–3016. [CrossRef] [PubMed]
13. Cai, L.; Kong, R.; Wang, Y.; Hu, H. Channel waveguides and y-junctions in x-cut single-crystal lithium niobate thin film. *Opt. Exp.* **2015**, *23*, 29211–29221. [CrossRef] [PubMed]
14. Cai, L.; Kang, Y.; Hu, H. Electric-optical property of the proton exchanged phase modulator in single-crystal lithium niobate thin film. *Opt. Exp.* **2016**, *24*, 4640–4647. [CrossRef]
15. Weigel, P.O.; Savanier, M.C.; DeRose, T.; Pomerene, A.T.; Starbuck, A.L.; Lentine, A.L.; Stenger, V.; Mookherjea, S. Lightwave circuits in lithium niobate through hybrid Waveguides with silicon photonics. *Sci. Rev.* **2016**, *6*, 22301. [CrossRef] [PubMed]

16. Volk, T.; Woehlecke, M. *Lithium Niobate: Defects, Photorefarction and Ferroelectric Switching*; Springer: Berlin and Heidelberg, Germany, 2008; ISBN: 978-3-540-70765-3.
17. Radojevic, A.M.; Levy, M.; Osgood, R.M., Jr.; Kumar, A.; Bakhru, H.; Tian, C.; Evans, C. Large etch-selectivity enhancement in the epitaxial liftoff of single-crystal $LiNbO_3$ films. *Appl. Phys. Lett.* **1999**, *74*, 3197–3199. [CrossRef]
18. Djukic, D.; Cerda-Pons, G.; Roth, R.M.; Osgood, R.M.; Bakhru, S.; Bakhru, H. Electro-optically tunable second-harmonic-generation gratings in ion-exfoliated thin films of periodically poled lithium niobate. *Appl. Phys. Lett.* **2007**, *90*, 171116. [CrossRef]
19. Gainutdinov, R.V.; Volk, T.R.; Zhang, H.H. Domain formation and polarization reversal under AFM-tip voltages in ion-sliced $LiNbO_3$ films on $SiO_2/LiNbO_3$ substrates. *Appl. Phys. Lett.* **2015**, *107*, 162903. [CrossRef]
20. Berger, V. Nonlinear photonic crystals. *Phys. Rev. Lett.* **1998**, *81*, 4136–4139. [CrossRef]
21. Shao, G.-H.; Bai, Y.-H.; Cui, G.-X.; Li, C.; Qiu, X.-B.; Geng, D.-Q.; Wu, D.; Lu, Y.-Q. Ferroelectric domain inversion and its stability in lithium niobate thin film on insulator with different thicknesses. *AIP Adv.* **2016**, *6*, 075011. [CrossRef]
22. Eng, L. Nanoscale domain engineering and characterization of ferroelectric domains. *Nanotech* **1999**, *10*, 405–411. [CrossRef]
23. Paruch, P.; Tybell, T.; Triscone, J.-M. Nanoscale control of ferroelectric polarization and domain size in epitaxial Pb.Zr0.2Ti0.8.O3 thin films. *Appl. Phys. Lett.* **2001**, *79*, 530–532. [CrossRef]
24. Cho, Y.; Fujimoto, K.; Hiranaga, Y.; Wagatsuma, Y.; Onoe, A.; Terabe, K.; Kitamura, K. Tbit/inch^{2}ferroelectric data storage based on scanning nonlinear dielectric microscopy. *Appl. Phys. Lett.* **2002**, *81*, 4401–4403. [CrossRef]
25. Daimon, Y.; Cho, Y. Cross-sectional observation of nanodomain dots formed in both congruent and stoichiometric $LiTaO_3$ crystals. *Appl. Phys. Lett.* **2007**, *90*, 192906. [CrossRef]
26. Kholkin, A.L.; Kalinin, S.V.; Roelofs, A.; Gruverman, A. Review of Ferroelectric Domain Imaging by Piezoresponse. Force Microscopy. In *Scanning Probe Microscopy Electrical and Electromechanical Phenomena at the Nanoscale*; Kalinin, S., Gruverman, A., Eds.; Springer: New York, NY, USA, 2007; ISBN-13: 978-0387-28667-9; ISBN-10: 0-387-28667-5.
27. Terabe, K.; Nakamura, M.; Takekawa, S.; Kitamura, K.; Higuchi, S.; Gotoh, Y.; Cho, Y. Microscale to nanoscale ferroelectric domain and surface engineering of a near-stoichiometric $LiNbO_3$ crystal. *Appl. Phys. Lett.* **2003**, *82*, 433–435. [CrossRef]
28. Rodriguez, B.J.; Nemanich, R.J.; Kingon, A.; Gruverman, A.; Kalinin, S.V.; Terabe, K.; Liu, X.Y.; Kitamura, K. Domain growth kinetics in lithium niobate single crystals studied by piezoresponse force microscopy. *Appl. Phys. Lett.* **2005**, *86*, 012906. [CrossRef]
29. Lilienblum, M.; Soergel, E. Anomalous domain inversion in $LiNbO_3$ single crystals investigated by scanning probe microscopy. *J. Appl. Phys.* **2011**, *110*, 052018. [CrossRef]
30. Tybell, T.; Paruch, P.; Giamarchi, T.; Triscone, J.-M. Domain wall creep in epitaxial ferroelectric $PbZr_{O.2}Ti_{0.8}O3$ thin films. *Phys. Rev. Lett.* **2002**, *89*, 097601. [CrossRef] [PubMed]
31. Kan, Y.; Bo, H.-F.; Lu, X.-M.; Xu, T.-T.; Jin, Y.M.; Wu, X.O.; Huang, F.Z.; Zhu, J.S. Decay properties of artificial two-domain structures in $LiNbO_3$ crystals studied by scanning probe microscope. *Appl. Phys. Lett.* **2010**, *97*, 202903. [CrossRef]
32. Ofan, A.; Lilienblum, M.; Gaathon, O.; Sehrbrock, A.; Hoffmann, Á.; Bakhru, S.; Bakhru, H.; Irsen, S R.; Osgood, M., Jr.; Soergel, E. Large-area regular nanodomain patterning in He-irradiated lithium niobate crystals. *Nanotech* **2011**, *22*, 285309. [CrossRef] [PubMed]
33. Ievlev, A.V.; Jesse, S.; Morozovska, A.N.; Strelcov, E.; Eliseev, E.A.; Pershin, Y.V.; Kumar, A.; Shur, V.Y.; Kalinin, S.V. Intermittency, quasiperiodicity and chaos in probe-induced ferroelectric domain switching. *Nat. Phys.* **2014**, *10*, 59–66. [CrossRef]
34. Seidel, J.; Martin, L.W.; He, Q.; Zhan, Q.; Chu, Y.-H.; Rother, A.; Hawkridge, M.E.; Maksymovych, P.; Yu, P.; Gajek, M.; et al. Conduction at domain walls in oxide multiferroics. *Nat. Mater.* **2009**, *8*, 229–234. [CrossRef] [PubMed]
35. Guyonnet, J.; Gaponenko, I.; Gariglio, S.; Paruch, P. Conduction at domain walls in insulating PZT thin films. *Adv. Mat.* **2011**, *23*, 5377–5382. [CrossRef] [PubMed]

36. Maksymovych, P.; Morozovska, A.N.; Yu, P.; Eliseev, E.A.; Chu, Y.-H.; Ramesh, R.; Baddorf, A.P.; Kalinin, S.V. Tunable metallic conductance in ferroelectric nanodomains. *Nanolett* **2012**, *12*, 209–213. [CrossRef] [PubMed]
37. Vasudevan, R.K.; Wu, W.; Guest, J.R.; Baddorf, A.P.; Morozovska, A.N.; Eliseev, E.A.; Balke, N.; Nagarajan, V.; Maksymovych, P.; Kalinin, S.V. Domain wall conduction and polarization-mediated transport in ferroelectrics. *Adv. Func. Mater.* **2013**, *23*, 2592–2616. [CrossRef]
38. Schroeder, M.; Haussmann, A.; Thiessen, A.; Soergel, E.; Woike, T.; Eng, L.M. Conducting domain walls in lithium niobate single crystals. *Adv. Funct. Mater.* **2012**, *22*, 3936–3944. [CrossRef]
39. Schroeder, M. Conductive Domain Walls in Ferroelectric Bulk Single Crystals. Ph.D. Thesis, Institut für Angewandte Physik Fakultät für Mathematik und Naturwissenschaften der Technischen Universität, Dresden, Germany, 2013.
40. Kaempfe, T.; Reichenbach, P.; Schroeder, M.; Haussmann, A.; Eng, L.M.; Woike, T.; Soergel, E. Optical three-dimensional profiling of charged domain walls in ferroelectrics by Cherenkov second-harmonic generation. *Phys. Rev. B* **2014**, *89*, 035314. [CrossRef]
41. Volk, T.R.; Gainutdinov, R.V.; Zhang, H.H. Domain-wall conduction in AFM-written domain patterns in ion-sliced $LiNbO_3$ films. *Appl. Phys. Lett.* **2017**, *110*, 132905. [CrossRef]
42. Eliseev, E.A.; Morozovska, A.N.; Svechnikov, G.S.; Gopalan, V.; Shur, V.Y. Static conductivity of charged domain walls in uniaxial ferroelectric semiconductors. *Phys. Rev. B* **2011**, *83*, 235313. [CrossRef]
43. Gonnissen, J.; Batuk, D.; Nataf, G.F.; Jones, L.; Abakumov, A.M.; Van Aert, S.; Schryvers, D.; Salje, E.K.H. Direct Observation of Ferroelectric Domain Walls in LiNbO3: Wall-Meanders, Kinks, and Local Electric Charges. *Adv. Funct. Mater.* **2016**. [CrossRef]